Editors' Suggestion

Temperature Dependence of Photoluminescence Intensity and Spin Contrast in Nitrogen-Vacancy Centers

S. Ernst,[1,*] P. J. Scheidegger,[1,*] S. Diesch,[1] L. Lorenzelli,[1] and C. L. Degen[1,2,†]
[1]Department of Physics, ETH Zurich, Otto Stern Weg 1, 8093 Zurich, Switzerland
[2]Quantum Center, ETH Zurich, 8093 Zurich, Switzerland

(Received 22 December 2022; accepted 9 May 2023; published 24 August 2023)

We report on measurements of the photoluminescence properties of single nitrogen-vacancy centers in diamond at temperatures between 4 K and 300 K. We observe a strong reduction of the PL intensity and spin contrast between ca. 10 K and 100 K that recovers to high levels below and above. Further, we find a rich dependence on magnetic bias field and crystal strain. We develop a comprehensive model based on spin mixing and orbital hopping in the electronic excited state that quantitatively explains the observations. Beyond a more complete understanding of the excited-state dynamics, our work provides a novel approach for probing electron-phonon interactions and a predictive tool for optimizing experimental conditions for quantum applications.

DOI: 10.1103/PhysRevLett.131.086903

The long coherence time [1] and the ease of optical spin readout have made the negatively charged nitrogen-vacancy (NV) center in diamond a preferred qubit for applications in quantum metrology [2] and quantum information [3]. Extraordinarily, the NV retains its quantum properties up to above room temperature, suggesting its use in both ambient and cryogenic environments. At room temperature, researchers have employed the NV's spin as a sensor for magnetic [4,5] and electric fields [6], and thermometry [7,8]. Cooled to below 10 K, spin-dependent optical transitions [9] have facilitated the implementation of prototypical quantum networks [10] and multiqubit quantum operations [11]. Additionally, cryogenic NV magnetometry has been performed at the micron [12] and nano scales [13,14].

While the photodynamics of NV centers at low temperature (below 10 K) and around room temperature have been studied in detail, the understanding in the intermediate temperature range is incomplete. Initial studies of the photoluminescence (PL) emission intensity of NV ensembles revealed a minimum around 25 K attributed to time averaging in the electronic excited state (ES) [15]. This averaging process is caused by phonon-mediated transitions between the two orbital branches [16,17]. A temperature-dependent reduction in PL intensity and spin contrast was also reported in connection with NV charge state instabilities [18]. Further, spin mixing in the ES due to magnetic field [19,20] or crystal strain [21] was identified as another mechanism for loss of PL. The strain-related spin mixing at low temperature was found to be partially mitigated by the application of a large magnetic bias field [15,20,22]. Because high PL intensity and spin contrast are essential for high-fidelity quantum readout and sensitive magnetometry, a complete picture of the NV photodynamics in the 10–100 K range is highly desirable.

In this Letter, we report measurements of the PL intensity and spin contrast for single NV centers between 4 K and 300 K. We show that a combination of orbital hopping and spin mixing in the ES leads to a strong reduction of both quantities between 10 K and 100 K. Based on measurements at varying magnetic field (0–200 mT) and intrinsic strain [ES splitting $2 \times (9\text{–}80)$ GHz], we develop a comprehensive theoretical model for the temperature-dependent dynamics of the ES. Details on the model and simulation framework are given in a companion paper [23]. As a result, we are able to quantitatively describe the NV's PL intensity and spin contrast over the complete parameter range of temperature, magnetic field, and strain, and we find excellent agreement with experimental data.

In our study, we investigate single NV centers situated in nanostructured pillars, which serve to enhance the photon collection efficiency. Our samples include an array of pillars on isotopically pure ^{12}C diamond (NV-1 to NV-4, ElementSix) and a scanning tip fabricated from natural-abundance material (NV-5, QZabre). NV centers are formed by shallow $^{15}N^+$ ion implantation (7 keV) followed by high-temperature annealing ($< 10^{-8}$ mbar, 880 °C, 2 h). Samples are measured in a dry dilution refrigerator (Setup A) at temperatures between 4 K and 100 K; an additional study down to 0.35 K did not show further variation in the NV behavior [24]. A second dry cryostat (Setup B) with a temperature range of 30–300 K is used to validate the aforementioned measurements and extend the range to room temperature [25]. Both setups operate in vacuum without the addition of exchange gas ($p < 5.5 \times 10^{-5}$ mbar). Magnetic bias fields, when specified, are applied along the NV symmetry axis.

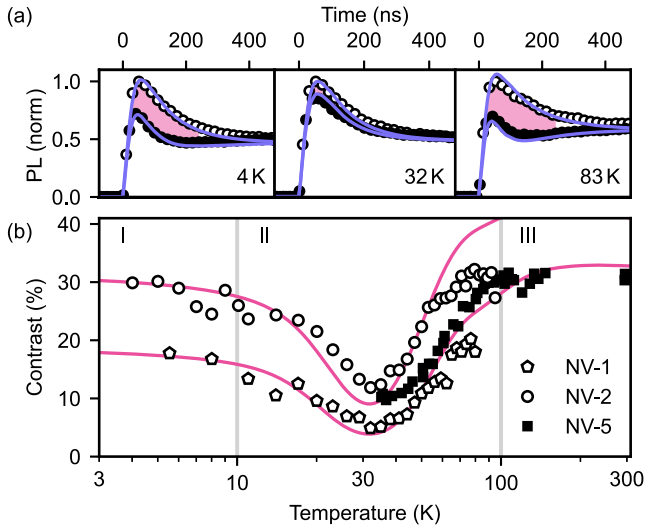

FIG. 1. (a) Time-dependent PL traces during a laser pulse, measured on NV-2 initialized to the $|0\rangle$ (open circles) and $|-1\rangle$ (filled circles) states at low, intermediate and high temperature. The spin contrast is given by the relative difference between the two curves (pink shading). Solid lines are fits to the PL dynamics. (b) Spin contrast versus temperature for three NV centers measured on Setup A (empty markers) and Setup B (filled marker). Solid lines show corresponding simulations for NV-1 and NV-2. A bias field of 3 mT is applied.

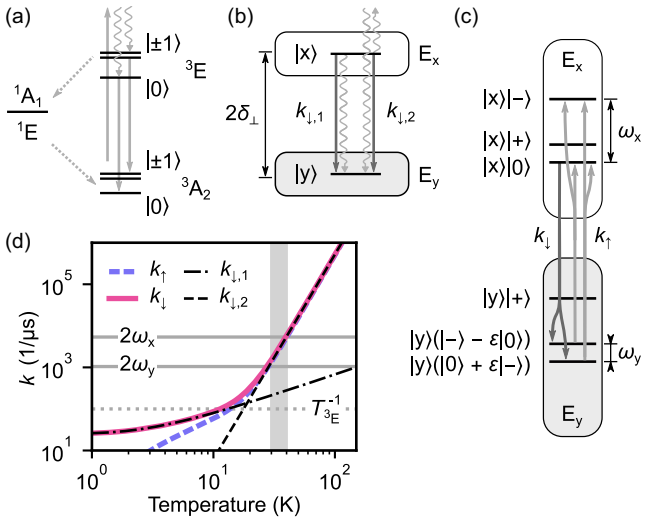

FIG. 2. (a) Level diagram in the NV spin subspace $\mathcal{H}_{\text{spin}}$ of the electronic ground ($^3A_2$) and excited (^3E) states, as well as the metastable ($^1A_1$, ^1E) shelving states. The intersystem crossing (dotted line) is spin selective, favoring decay out of $|\pm1\rangle$. In panels (a)–(c), solid arrows mark spin-conserving transitions, and curly arrows symbolize phonons. (b) Level diagram in the orbital subspace $\mathcal{H}_{\text{orbit}}$ of the NV ES (^3E). Two orbital branches (E_x, E_y) split under strain $\delta_\perp$. One- and two-phonon processes cause hopping between branches at temperature-dependent rates $k_{\downarrow,1(2)}$ ($k_{\uparrow,1(2)}$ not shown). (c) Example of levels in the composite Hilbert space of orbit and spin $\mathcal{H}_{\text{orbit}} \otimes \mathcal{H}_{\text{spin}}$. Eigenstates are superpositions of $|0\rangle$ and $|\pm\rangle \propto (|+1\rangle \pm |-1\rangle)$. Spin-conserving, phonon-mediated transitions involving $|0\rangle$ are depicted by gray arrows. $\omega_{x(y)}$ are the Larmor frequencies of involved spin transitions. (d) Hopping rates as a function of temperature. Inverse optical lifetime $T_{^3E}^{-1}$ and Larmor frequencies (in MHz) are indicated by horizontal lines. For panels (c) and (d), we use $\delta_\perp = 40$ GHz in the direction of a carbon bond at low magnetic field, such that only two basis states mix significantly ($|\varepsilon|^2 = |\epsilon_{|y,0\rangle,|y,-\rangle}|^2 = 0.1$ [26]).

The central experimental observation of this Letter is reported in Fig. 1, which plots the spin contrast as a function of temperature $T = 4$–300 K. The PL intensity follows a similar trend (see Fig. S7 in the Supplemental Material [26]), but it is more prone to experimental drift. We measure the contrast by integrating the relative difference in PL between the $m_S = 0$ and $m_S = -1$ states (subsequently denoted by $|0\rangle$ and $|-1\rangle$) during the first 250 ns under excitation with a 520 nm diode laser [Fig. 1(a)]. To initialize the spin state into $|0\rangle$, we use a 2 μs laser pulse, followed by a state swap to $|-1\rangle$ (when needed) using an adiabatic inversion microwave pulse [27]. Figure 1(b) clearly reveals three temperature regimes: (I) Below ca. 10 K, the spin contrast is mostly constant. (II) Between ca. 10 K and 100 K, the spin contrast is strongly reduced with a pronounced minimum around 35 K and then recovers for higher temperatures. (III) Above ca. 100 K, the spin contrast remains approximately constant up to room temperature. In all measurements, the room-temperature contrast exceeds the low-temperature limit. At even higher temperatures, the contrast has been shown to slowly decrease until it vanishes around 700 K [28].

Before providing a theoretical explanation for the behavior seen in Fig. 1, we briefly recall the mechanism for contrast generation by looking at the spin subspace of the NV given in Fig. 2(a) [29]. After spin-conserving optical excitation from the ground state (GS) into the ES, a spin-selective intersystem crossing (ISC) leads to preferential population of the shelving state for $|\pm1\rangle$. Because the shelving state ^1E has a relatively long lifetime, the average PL emission is lower for $|\pm1\rangle$ compared to $|0\rangle$, leading to spin contrast. The PL reduction is temporary and disappears due to optical repumping into $|0\rangle$ after a few hundred nanoseconds [see Fig. 1(a)]. Crucially, this mechanism of contrast generation is effective only for as long as there are no transitions between the ES spin states.

We next consider the orbital subspace of the NV ES (^3E), which is a doublet shown in Fig. 2(b) [29]. In the presence of in-plane strain $\delta_\perp$ relative to the NV principal axis, the ES possesses two orbital branches, E_x and E_y, split by $2\delta_\perp$ [30]. In the composite space of orbit and spin, each branch has three spin states, leading to a total of six energy eigenlevels [Fig. 2(c)]. We now show that the contrast reduction and recovery can be explained by the interplay of two mechanisms: spin mixing and orbital branch hopping in the ES.

First, we discuss the effects of spin mixing, meaning that the ES eigenstates are not pure spin eigenstates. As an

example, we consider Fig. 2(c). Here, the $|0\rangle$ state is in good approximation an eigenstate of the E_x branch but not of the E_y branch, where it forms a superposition with the $|-\rangle \propto (|+1\rangle - |-1\rangle)$ state. Consequently, optical excitation into the E_x branch is spin conserving, while excitation into the E_y branch will lead to spin mixing. In general, the spin-mixing amplitudes $\epsilon_{|i\rangle,|j\rangle}$ between basis states $|i\rangle$ and $|j\rangle$ in the six eigenlevels depend on the strain magnitude and direction [21,31], as well as magnetic field alignment [19] and magnitude [20]. Therefore, the spin contrast is both strain- and field-dependent. Although the $\epsilon_{|i\rangle,|j\rangle}$'s are typically small, they play a key role in the mechanism of spin relaxation.

Second, we consider the effects of orbital hopping, which refers to spin-conserving transitions between E_x and E_y driven by phonons. Figure 2(b) schematically depicts the dominant contributions arising from one-phonon processes (rates k_1) and two-phonon processes (rates k_2) derived in Refs. [23,32,33]. The one-phonon downward ($E_x \to E_y$) hopping rate is given by

$$k_{\downarrow,1}(T,\delta_\perp) \propto \eta\delta_\perp^3[n(2h\delta_\perp/k_B T)+1], \tag{1}$$

where η parametrizes the electron-phonon coupling and n is the Bose-Einstein distribution function. The rate of the two-phonon process is given by

$$k_{\downarrow,2}(T) \propto \eta^2 T^5 I(T), \tag{2}$$

where $I(T)$ is a mildly strain- and temperature-dependent integral over the phonon spectrum that we solve in the Debye approximation. The total hopping rates are the sums of the one- and two-phonon contributions, $k_{\downarrow(\uparrow)} = k_{\downarrow(\uparrow),1} + k_{\downarrow(\uparrow),2}$. The upward ($E_y \to E_x$) rate significantly differs from the downward rate only below 10 K, where it is reduced by the absence of spontaneous emission [the second term in Eq. (1)]. Figure 2(d) plots the hopping rates for the parameters in Fig. 2(c) as a function of temperature. It provides the key to explaining our experimental observations in the temperature regimes (I–III): (I) Below ca. 10 K, the orbital hopping is dominated by $k_{\downarrow,1}$ due to the spontaneous emission. Since $k_{\downarrow,1}$ is slower than the ES decay rate ($T_{^3E}^{-1} \approx 10^8\ s^{-1}$) for typical strain values $\delta_\perp \lesssim 40$ GHz, the ES spin states are mostly preserved (except for some small spin mixing $\epsilon_{|i\rangle,|j\rangle}$), and the spin contrast is high. (II) Above 10 K, the two-phonon process starts to dominate. Once $k > T_{^3E}^{-1}$, spin relaxation between $|0\rangle$ and $|\pm 1\rangle$ is drastically amplified, because the time evolution under different Larmor precession in both branches becomes randomized by the frequent hopping. This relaxation mechanism is most efficient when a hopping event occurs approximately every half of a Larmor precession period $(2\omega_{x(y)})^{-1}$ [23]. This occurs between ca. 30 K and 40 K [gray shading in Fig. 2(d)] and coincides with the temperature where we observe the strongest suppression of the spin contrast. (III) As the temperature increases further, the orbital hopping rates become much faster than the spin dynamics, and the two orbital states are time averaged [15,30]. This effectively renders ^3E an orbital singlet similar to the GS $^3A_2$ [34] and leads to the commonly accepted room-temperature model appearing as in Fig. 2(a). Since $|0\rangle$ and $|\pm 1\rangle$ are pure eigenstates of the time-averaged Hamiltonian, the highest spin contrast is observed in this regime.

Armed with this theory, we implement a rate model to quantitatively reproduce the experimental observations by numerical simulations. Details on the rate model and simulations are given in a companion paper [23] and the Supplemental Material [26], which includes Refs. [35–42]. We model the orbital hopping by spin-conserving Markovian transitions between the two orbital branches. Since spin coherences are maintained during the transitions, we use a Lindblad master equation rather than a classical rate model. We describe the ES in a composite Hilbert space of spin and orbit ($\mathcal{H}_{ES} = \mathcal{H}_{orbit} \otimes \mathcal{H}_{spin}$) and formulate the spin-conserving jump operators as

$$L_\downarrow^{ES} = \sqrt{k_{\downarrow,1}+k_{\downarrow,2}}|y\rangle\langle x| \otimes \mathbb{I}_3, \tag{3}$$

and likewise for $L_\uparrow^{ES}$. We further introduce optical excitation, decay, and ISC by classical jump operators. The resulting Liouville equation describes the time evolution of the ten-dimensional density matrix $\rho(t)$, containing three GS levels, six ES levels, and one combined shelving state.

To simulate the behavior of a chosen NV center, we feed our model with values obtained from a simultaneous fit of three sets of calibration measurements: (i) We use a measurement of the steady-state PL intensity as a function of magnetic field at base temperature [see Fig. 3(b) at 4 K] to obtain strain values and unintended misalignment of the bias field, by fitting the minima in the PL at level anticrossings [15,20]. (ii) We pick a set of 24 time-dependent PL traces [cf. Fig. 1(a)], including two spin states ($|0\rangle$, $|-1\rangle$), six temperatures (4–100 K), and low and high bias fields (3 mT, 200 mT). Fits to these PL traces then yield the optical decay and ISC rates, which are approximately temperature independent [43] and are known to vary between NV centers [29,44], as well as the coupling strength η. We determine the shelving state lifetime [31,44], which has a mild, well-known temperature dependence, in a separate calibration. (iii) For each time-dependent PL trace, we perform an optical saturation measurement to quantify drift in the background luminescence, optical alignment, and ratio of collection over excitation efficiency. Finally, we use literature values for the NV fine structure [45,46].

As an important side result, our calibration yields values for the electron-phonon couplings η ranging

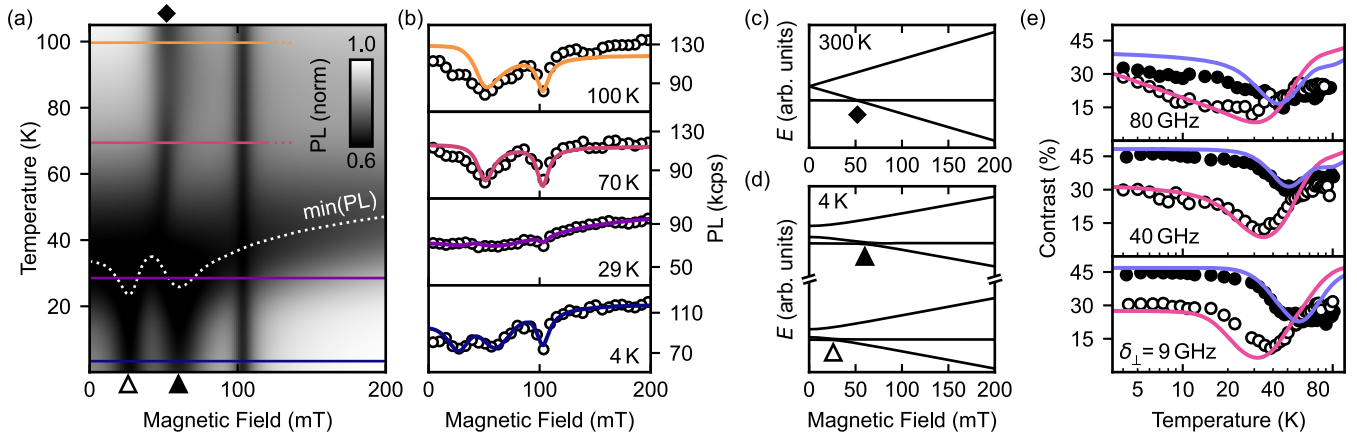

FIG. 3. (a) Simulation of the PL in dependence of the magnetic field and temperature. The PL is strongly reduced at avoided crossings of the excited-state (symbols) and the ground-state (103 mT) energy levels. The white dotted line marks the PL minimum; colored solid lines indicate the line cuts shown in panel (b). The simulation is based on parameters fitted to NV-1. (b) Experimental PL curves for NV-1 measured as a function of magnetic field and temperature. Solid lines are fits. (c),(d) Energy levels for the NV-1 ES at 300 K (c, time-averaged) and at 4 K (d). Symbols refer to panel (a). (e) Experimental spin contrast as a function of temperature for NV centers with different strain $\delta_\perp$. Measurements are taken at 3 mT (empty circles) and 200 mT (filled circles). Solid lines show the corresponding simulations.

from 176 $\mu s^{-1}\,meV^{-3}$ [NV-2, used in Fig. 2(d)] to 268 $\mu s^{-1}\,meV^{-3}$ (NV-4), in good agreement with Refs. [17,32,33]. We note that these studies use different phonon models in the evaluation of $I(T)$. While our data does not allow validation of a particular model with certainty, our measurement approach provides complementary insight into $I(T)$ [23,26].

We are now ready to return to Fig. 1(b) and use our model and calibration to simulate the temperature-dependent PL and spin contrast (solid curves). Overall, we find an excellent agreement between experimental and simulated results. In particular, the model quantitatively reproduces all temperature regimes (I–III), including the minimum in contrast around 35 K and the recovery toward room temperature. Although the agreement is not perfect at elevated temperatures, which we attribute to setup instabilities and uncertainty in temperature calibration [26], our model successfully bridges the classical rate models used in the limits of low [20] and high [19,44] temperatures.

Next, we use our model to predict the PL properties as a function of magnetic bias field. In Figs. 3(a) and 3(b), we plot the simulated PL intensity as a function of $B = 0$–200 mT and $T = 0$–100 K together with the experimental results. The model successfully predicts the known reductions in PL (indicated by symbols) at magnetic fields that correspond to level anticrossings (LACs) in the ES, in both the low- [Fig. 3(d)] and high-temperature limits [Fig. 3(c), obtained from Fig. 3(d) by a partial trace over the orbital subspace]. The global PL minimum—indicated by the dotted line in Fig. 3(a)—depends on the exact energy level spacing at a given magnetic field (and strain). For example, we observe that with increasing magnetic field (beyond the second ES LAC), the PL minimum becomes less pronounced and shifts to higher temperatures. This behavior is readily explained by a lower degree of spin mixing in the eigenstates [smaller $\epsilon_{|i\rangle,|j\rangle}$ in Fig. 2(c)] and higher Larmor frequencies [larger $\omega_{x(y)}$ in Fig. 2(d)] at high field. However, even at the highest field accessible in our experiment (200 mT), the PL minimum is still noticeable. Full recovery of the PL is expected for fields significantly above 1 T (see Fig. S10 in the Supplemental Material [26]).

Finally, we examine the influence of crystal strain. In Fig. 3(e), we compare the temperature dependence of the spin contrast for NV centers with high (NV-4, 80 GHz), medium (NV-2, 40 GHz), and low (NV-3, 9 GHz) intrinsic strain within our accessible range (NV-1 has 32 GHz). While all curves show the same qualitative behavior, we find that the most prominent feature is a decrease in the spin contrast at high strain $\delta_\perp$ already below 10 K. This feature can be understood through the factor $\delta_\perp^3$ in Eq. (1): $k_{\uparrow,1}$ is rapidly increasing as the required high-energy phonon modes become thermally activated, approaching $k_{\downarrow,1}$, which is generally high due to spontaneous emission (see Fig. S11 in the Supplemental Material [26]).

In conclusion, we developed a rate model that explains the NV center photophysics over a broad range of temperature, magnetic bias field, and crystal strain. We find excellent agreement with experiments. In particular, our model successfully predicts a minimum in the PL emission and spin contrast around 35 K due to rapid spin relaxation driven by an interplay of spin mixing and orbital hopping. This spin relaxation process degrades both the spin initialization and the spin readout fidelity (see Fig. S9 in the Supplemental Material [26]). It is of fundamental nature and universal to all NV centers, including NV centers deep

in the bulk that experience negligible crystal strain [30] (see Fig. S10 in the Supplemental Material [26]).

Our work provides useful insight beyond giving a more complete picture of the NV excited-state dynamics. First, our model can account for the observed temperature dependence by phonon-induced processes in the ES alone. Therefore, we conclude that charge-state switching between NV^- and NV^0 does not play a key role in explaining the spin contrast as a function of temperature. We also have not observed any signs of charge state instabilities on the few-minutes timescale of our measurements (see Fig. S2 in the Supplemental Material [26]). Second, our work introduces a new measurement approach for probing electron-phonon interactions and contributing modes, applicable in regimes where resonant laser PL excitation spectroscopy [32] or measurement of motional narrowing on ES ODMR lines [33] are unavailable. Third, we examined the rich dependence on magnetic field, strain (or equivalently electric field [29]), and temperature. Here, our model offers a predictive tool for maximizing the PL intensity and spin contrast, which are the key quantities for achieving high spin readout fidelity and high metrology sensitivity in quantum applications.

The authors thank Matthew Markham (ElementSix) for providing the ^{12}C diamond and Jan Rhensius (QZabre) for nanofabrication. We thank Erika Janitz, Fedor Jelezko, Assaf Hamo, Konstantin Herb, William Huxter, Patrick Maletinsky, Francesco Poggiali, Friedemann Reinhard, Jörg Wrachtrup, and Jonathan Zopes for useful input and discussions. This work was supported by the European Research Council through ERC CoG 817720 (IMAGINE), the Swiss National Science Foundation (SNSF) through Project Grant No. 200020_175600, and through the NCCR QSIT, a National Centre of Competence in Research in Quantum Science and Technology, Grant No. 51NF40-185902, and the Advancing Science and TEchnology thRough dIamond Quantum Sensing (ASTERIQS) program, Grant No. 820394, of the European Commission.

Note added.—We acknowledge related work on the temperature dependence of the NV photophysics by Blakley *et al.* [47] and Happacher *et al.* [48].

*These authors contributed equally to this work.
†degenc@ethz.ch

[1] E. D. Herbschleb, H. Kato, Y. Maruyama, T. Danjo, T. Makino, S. Yamasaki, I. Ohki, K. Hayashi, H. Morishita, M. Fujiwara, and N. Mizuochi, Ultra-long coherence times amongst room-temperature solid-state spins, Nat. Commun. **10**, 3766 (2019).

[2] R. Schirhagl, K. Chang, M. Loretz, and C. L. Degen, Nitrogen-vacancy centers in diamond: Nanoscale sensors for physics and biology, Annu. Rev. Phys. Chem. **65**, 83 (2014).

[3] L. Childress and R. Hanson, Diamond NV centers for quantum computing and quantum networks, MRS Bull. **38**, 134 (2013).

[4] J. R. Maze, P. L. Stanwix, J. S. Hodges, S. Hong, J. M. Taylor, P. Cappellaro, L. Jiang, M. V. G. Dutt, E. Togan, A. S. Zibrov, A. Yacoby, R. L. Walsworth, and M. D. Lukin, Nanoscale magnetic sensing with an individual electronic spin in diamond, Nature (London) **455**, 644 (2008).

[5] G. Balasubramanian, I. Y. Chan, R. Kolesov, M. Al-Hmoud, J. Tisler, C. Shin, C. Kim, A. Wojcik, P. R. Hemmer, A. Krueger, T. Hanke, A. Leitenstorfer, R. Bratschitsch, F. Jelezko, and J. Wrachtrup, Nanoscale imaging magnetometry with diamond spins under ambient conditions, Nature (London) **455**, 648 (2008).

[6] F. Dolde, H. Fedder, M. W. Doherty, T. Noebauer, F. Rempp, G. Balasubramanian, T. Wolf, F. Reinhard, L. C. L. Hollenberg, F. Jelezko, and J. Wrachtrup, Electric-field sensing using single diamond spins, Nat. Phys. **7**, 459 (2011).

[7] G. Kucsko, P. C. Maurer, N. Y. Yao, M. Kubo, H. J. Noh, P. K. Lo, H. Park, and M. D. Lukin, Nanometre-scale thermometry in a living cell, Nature (London) **500**, 54 (2013).

[8] V. M. Acosta, E. Bauch, M. P. Ledbetter, A. Waxman, L. S. Bouchard, and D. Budker, Temperature Dependence of the Nitrogen-Vacancy Magnetic Resonance in Diamond, Phys. Rev. Lett. **104**, 070801 (2010).

[9] L. Robledo, L. Childress, H. Bernien, B. Hensen, P. F. A. Alkemade, and R. Hanson, High-fidelity projective read-out of a solid-state spin quantum register, Nature (London) **477**, 574 (2011).

[10] M. Pompili, S. L. N. Hermans, S. Baier, H. K. C. Beukers, P. C. Humphreys, R. N. Schouten, R. F. L. Vermeulen, M. J. Tiggelman, L. dos Santos Martins, B. Dirkse, S. Wehner, and R. Hanson, Realization of a multinode quantum network of remote solid-state qubits, Science **372**, 259 (2021).

[11] C. E. Bradley, J. Randall, M. H. Abobeih, R. C. Berrevoets, M. J. Degen, M. A. Bakker, M. Markham, D. J. Twitchen, and T. H. Taminiau, A Ten-Qubit Solid-State Spin Register with Quantum Memory up to One Minute, Phys. Rev. X **9**, 031045 (2019).

[12] S. E. Lillie, D. A. Broadway, N. Dontschuk, S. C. Scholten, B. C. Johnson, S. Wolf, S. Rachel, L. C. L. Hollenberg, and J.-P. Tetienne, Laser modulation of superconductivity in a cryogenic wide-field nitrogen-vacancy microscope, Nano Lett. **20**, 1855 (2020).

[13] T. Song, Q. C. Sun, E. Anderson, C. Wang, J. Qian, T. Taniguchi, K. Watanabe, M. A. McGuire, R. Stohr, D. Xiao, T. Cao, J. Wrachtrup, and X. Xu, Direct visualization of magnetic domains and Moire magnetism in twisted 2D magnets, Science **374**, 1140 (2021).

[14] L. Thiel, Z. Wang, M. A. Tschudin, D. Rohner, I. Gutierrez-lezama, N. Ubrig, M. Gibertini, E. Giannini, A. F. Morpurgo, and P. Maletinsky, Probing magnetism in 2D materials at the nanoscale with single-spin microscopy, Science **364**, 973 (2019).

[15] L. J. Rogers, R. L. Mcmurtrie, M. J. Sellars, and N. B. Manson, Time-averaging within the excited state of the nitrogen-vacancy centre in diamond, New J. Phys. **11**, 063007 (2009).

[16] K. C. Fu, C. Santori, P. E. Barclay, L. J. Rogers, N. B. Manson, and R. G. Beausoleil, Observation of the Dynamic Jahn-Teller Effect in the Excited States of Nitrogen-Vacancy Centers in Diamond, Phys. Rev. Lett. **103**, 256404 (2009).

[17] T. A. Abtew, Y. Y. Sun, B. C. Shih, P. Dev, S. B. Zhang, and P. Zhang, Dynamic Jahn-Teller Effect in the NV^- Center in Diamond, Phys. Rev. Lett. **107**, 146403 (2011).

[18] D. F. Wise, Could NV centres in diamond be used to measure donor spins in silicon?, Ph.D. thesis, University College London, London, 2021.

[19] J. Tetienne, L. Rondin, P. Spinicelli, M. Chipaux, T. Debuisschert, J. Roch, and V. Jacques, Magnetic-field-dependent photodynamics of single NV defects in diamond: An application to qualitative all-optical magnetic imaging, New J. Phys. **14**, 103033 (2012).

[20] J. Happacher, D. A. Broadway, J. Bocquel, P. Reiser, A. Jimenéz, M. A. Tschudin, L. Thiel, D. Rohner, M. l. G. Puigibert, B. Shields, J. R. Maze, V. Jacques, and P. Maletinsky, Low-Temperature Photophysics of Single Nitrogen-Vacancy Centers in Diamond, Phys. Rev. Lett. **128**, 177401 (2022).

[21] P. Tamarat, N. B. Manson, J. P. Harrison, R. L. McMurtrie, A. Nizovtsev, C. Santori, R. G. Beausoleil, P. Neumann, T. Gaebel, F. Jelezko, P. Hemmer, and J. Wrachtrup, Spin-flip and spin-conserving optical transitions of the nitrogen-vacancy centre in diamond, New J. Phys. **10**, 045004 (2008).

[22] U. Vool, A. Hamo, G. Varnavides, Y. Wang, T. X. Zhou, N. Kumar, Y. Dovzhenko, Z. Qiu, C. A. C. Garcia, A. T. Pierce, J. Gooth, P. Anikeeva, C. Felser, P. Narang, and A. Yacoby, Imaging phonon-mediated hydrodynamic flow in WTe_2, Nat. Phys. **17**, 1216 (2021).

[23] S. Ernst, P. J. Scheidegger, S. Diesch, and C. L. Degen, companion paper, Modeling temperature-dependent population dynamics in the excited state of the nitrogen-vacancy center in diamond, Phys. Rev. B, **108**, 085203 (2023).

[24] P. J. Scheidegger, S. Diesch, M. L. Palm, and C. L. Degen, Scanning nitrogen-vacancy magnetometry down to 350 mK, Appl. Phys. Lett. **120**, 224001 (2022).

[25] L. Lorenzelli, Development of a scanning nitrogen-vacancy-center magnetometer for variable temperature experiments, Ph.D. thesis, ETH Zurich, Zurich, 2021.

[26] See Supplemental Material at http://link.aps.org/supplemental/10.1103/PhysRevLett.131.086903 accompanying this manuscript.

[27] E. Kupce and R. Freeman, Adiabatic pulses for wideband inversion and broadband decoupling, J. Magn. Reson., Ser. A **115**, 273 (1995).

[28] D. M. Toyli, D. J. Christle, A. Alkauskas, B. B. Buckley, C. G. van de Walle, and D. D. Awschalom, Measurement and Control of Single Nitrogen-Vacancy Center Spins above 600 K, Phys. Rev. X **2**, 031001 (2012).

[29] M. W. Doherty, N. B. Manson, P. Delaney, F. Jelezko, J. Wrachtrup, and L. C. Hollenberg, The nitrogen-vacancy colour centre in diamond, Phys. Rep. **528**, 1 (2013).

[30] A. Batalov, V. Jacques, F. Kaiser, P. Siyushev, P. Neumann, L. J. Rogers, R. L. McMurtrie, N. B. Manson, F. Jelezko, and J. Wrachtrup, Low Temperature Studies of the Excited-State Structure of Negatively Charged Nitrogen-Vacancy Color Centers in Diamond, Phys. Rev. Lett. **102**, 195506 (2009).

[31] N. B. Manson, J. P. Harrison, and M. J. Sellars, Nitrogen-vacancy center in diamond: Model of the electronic structure, Phys. Rev. B **74**, 104303 (2006).

[32] M. L. Goldman, A. Sipahigil, M. W. Doherty, N. Y. Yao, S. D. Bennett, M. Markham, D. J. Twitchen, N. B. Manson, A. Kubanek, and M. D. Lukin, Phonon-Induced Population Dynamics and Intersystem Crossing in Nitrogen-Vacancy Centers, Phys. Rev. Lett. **114**, 145502 (2015).

[33] T. Plakhotnik, M. W. Doherty, and N. B. Manson, Electron-phonon processes of the nitrogen-vacancy center in diamond, Phys. Rev. B **92**, 081203(R) (2015).

[34] T. Plakhotnik, M. W. Doherty, J. H. Cole, R. Chapman, and N. B. Manson, All-optical thermometry and thermal properties of the optically detected spin resonances of the NV-center in nanodiamond, Nano Lett. **14**, 4989 (2014).

[35] R. Ulbricht, S. Dong, I. Chang, B. M. K. Mariserla, K. M. Dani, K. Hyeon-Deuk, and Z. Loh, Jahn-Teller-induced femtosecond electronic depolarization dynamics of the nitrogen-vacancy defect in diamond, Nat. Commun. **7**, 13510 (2016).

[36] D. Wirtitsch, G. Wachter, S. Reisenbauer, M. Gulka, V. Ivády, F. Jelezko, A. Gali, M. Nesladek, and M. Trupke, Exploiting ionization dynamics in the nitrogen vacancy center for rapid, high-contrast spin, and charge state initialization, Phys. Rev. Res. **5**, 013014 (2023).

[37] M. L. Goldman, M. W. Doherty, A. Sipahigil, N. Y. Yao, S. D. Bennett, N. B. Manson, A. Kubanek, and M. D. Lukin, State-selective intersystem crossing in nitrogen-vacancy centers, Phys. Rev. B **91**, 165201 (2015); **96**, 039905(E) (2017).

[38] A. Gali, *Ab initio* theory of the nitrogen-vacancy center in diamond, Nanophotonics **8**, 1907 (2019).

[39] A. Dreau, M. Lesik, L. Rondin, P. Spinicelli, O. Arcizet, J. F. Roch, and V. Jacques, Avoiding power broadening in optically detected magnetic resonance of single NV defects for enhanced dc magnetic field sensitivity, Phys. Rev. B **84**, 195204 (2011).

[40] D. A. Hopper, H. J. Shulevitz, and L. C. Bassett, Spin readout techniques of the nitrogen-vacancy center in diamond, Micromachines **9**, 437 (2018).

[41] A. Gupta, L. Hacquebard, and L. Childress, Efficient signal processing for time-resolved fluorescence detection of nitrogen-vacancy spins in diamond, J. Opt. Soc. Am. B **33**, B28 (2016).

[42] N. Kalb, P. C. Humphreys, J. J. Slim, and R. Hanson, Dephasing mechanisms of diamond-based nuclear-spin memories for quantum networks, Phys. Rev. A **97**, 062330 (2018).

[43] M. L. Goldman, M. W. Doherty, A. Sipahigil, N. Y. Yao, S. D. Bennett, N. B. Manson, A. Kubanek, and M. D. Lukin, State-selective intersystem crossing in nitrogen-vacancy centers, Phys. Rev. B **91**, 165201 (2015).

[44] L. Robledo, H. Bernien, T. van der Sar, and R. Hanson, Spin dynamics in the optical cycle of single nitrogen-vacancy centres in diamond, New J. Phys. **13**, 025013 (2011).

[45] L. C. Bassett, F. J. Heremans, D. J. Christle, C. G. Yale, G. Burkard, B. B. Buckley, and D. D. Awschalom, Ultrafast optical control of orbital and spin dynamics in a solid-state defect, Science **345**, 1333 (2014).

[46] X. D. Chen, C. H. Dong, F. W. Sun, C. L. Zou, J. M. Cui, Z. F. Han, and G. C. Guo, Temperature dependent energy level shifts of nitrogen-vacancy centers in diamond, Appl. Phys. Lett. **99**, 161903 (2011).

[47] S. M. Blakley, T. T. Mai, S. J. Moxim, J. T. Ryan, A. J. Biacchi, A. R. H. Walker, and R. D. McMichael, Spectroscopy of photoionization from the ^{1}E singlet state in nitrogen-vacancy centers in diamond, arXiv:2301.10383.

[48] J. Happacher, J. Bocque, H. T. Dinani, M. A. Tschudin, P. Reiser, D. A. Broadway, J. R. Maze, and P. Maletinsky, following Letter, Temperature-Dependent Photophysics of Single NV Centers in Diamond, Phys. Rev. Lett. **131**, 086904 (2023).